Post-print version of the paper by Wang et al. in Dental Materials, 35 (2019) 1254-1263.

https://doi.org/10.1016/j.dental.2019.05.022

High strength polymer/silicon nitride composites for dental restorations

Abstract

Objectives. To fabricate polymer-infiltrated silicon nitride composite (PISNC) and evaluate the potential of PISNC in dental application.

Methods. Porous silicon nitride (Si_3N_4) ceramics were fabricated through gelcasting and pressureless sintering. Polymer infiltrating was carried out then and composites were obtained after curing of polymer. Flexural strength and microstructures of porous ceramic scaffolds and polymer-infiltrated composites were obtained by three-point bending and SEM, respectively. Phase distributions of polymer-infiltrated ceramics were observed by EDS. Human gingival fibroblast cells (HGFs) were used to evaluate the cytocompatibility and IL-6 release. The cell morphology were observed by SEM. The amount of released IL-6 was investigated using ELISA test system.

Results. Porosity and mechanical strength of porous ceramics ranged from 45.1-49.3% and 171.8-262.3MPa, respectively. The bicontinuous structure of polymer-infiltrated composites possessed them with excellent mechanical properties. Porosity and mechanical strength of polymer-infiltrated Si_3N_4 composites ranged from 1.94-2.28% and 273-385.3MPa, respectively. Additionally, the PISNC enhanced the initial adhesion and spreading activity of HGFs compared with PMMA. The PISNC

showed similar IL-6 release performance with PMMA sample.

Significances. The PISNC is a promising candidate for dental restorations and high-load medical applications.

Keywords: Porous Si_3N_4; Polymer-infiltrated Si_3N_4 composites; Dental restoration; Cytocompatibility.

1. Introduction

Silicon nitride (Si_3N_4) ceramics possess excellent properties such as high strength, hardness, wear resistance and thermal shock resistance [1-3], which lead to wide applications of Si_3N_4 ceramics as bearings, heat engine components, cutting tools, hot gas filters, radome materials, and so on [3-5]. Recently, silicon nitride (Si_3N_4) based ceramics have attracted more and more attention in biomedical fields due to their inherent bioinert characteristic and good biocompatibility. The possibility of using silicon nitride ceramics for structural orthopaedic implants has been well explored and proved by Mauro Mazzocchi et al. [6, 7]. And diamond-like carbon (DLC) modified Si_3N_4 ceramics has been proved to be well adequate for articular prostheses medical application [8]. Zahi et al. also suggest Si_3N_4 implants as a promising choice in dental implantology [9]. However, all-ceramic restoration of Si_3N_4 ceramics may result in excessive wear of opposing teeth. Ceramic-polymer composite strategy is considered as an effective way to improve the comprehensive performance of all-ceramic restorations.

Composites of polymer and ceramic are expected to combine advantages of both components. Comparing with mono-phase polymers or ceramics, polymer-ceramic

composites are likely to achieve an elastic modulus similar to natural bone tissue. However, it seems that polymer-based composites always show low strength and low toughness, which restrict their wide applications. Generally, polymer-ceramic composites fabricated by dispersing ceramic particles in polymer matrixes can improve the strength of polymers to some extent [10, 11]. While the mechanical properties of polymers limit the final mechanical properties of polymer-ceramic composites since the polymer phase provide a continuous network in this case. A new way that can effectively improve the mechanical properties of resin-ceramic composites has been reported recently. This method creates a bicontinuous network which contains a porous ceramic structure and an interpenetrated polymer phase [12, 13]. The porous ceramic skeletons can provide the composites with high strength and moderate hardness. In this case, both inorganic and organic phases are continuous in the composites. Thus, the advantages of organic and inorganic part can be utilized to the most.

Si_3N_4 ceramic with elongated grains is supposed to be an excellent candidate of porous matrix. High strength porous Si_3N_4 ceramics with moderate porosity can be obtained through gelcasting with IBMA (copolymer of isobutylene and maleic anhydride) and pressureless sintering [14]. By infiltrating polymer into high strength porous Si_3N_4 skeletons, bicontinuous ceramic-polymer composites with excellent mechanical strength can be fabricated. Which can broaden the use of Si_3N_4 ceramics in high load-bearing medical applications, especially in dental applications.

In present work, porous Si_3N_4 scaffolds with various porosity were fabricated

through gel casting method from suspensions with different solid content. Bicontinuous PISNCs were then fabricated by infiltrating PMMA resin into porous scaffolds followed by a polymerization process. Microstructure, mechanical performance of the porous ceramic matrix and PISNCs were investigated. The cytocompatibility of PISNCs were also compared with PMMA and Si_3N_4 ceramics.

2. Experimental procedure

2.1 Fabrication of polymer-infiltrated Si_3N_4 composites

Porous Si_3N_4 ceramics were fabricated through gelcasting and liquid-phase sintering. Si_3N_4 powder (α-phase ≥ 95wt%; d_{50}=0.5μm; Ube Industries Ltd., Japan), Y_2O_3 powder (5.0 μm; purity ≥ 99.99wt%; Yuelong Company, Shanghai, China) and copolymer of isobutylene and maleic anhydride (IBMA, Isobam104#, Kuraray Co., Ltd., Osaka, Japan) were added into distilled water and milled with Si_3N_4 balls for 2.5h at a rotating speed of 350 r/min. Solid content of the suspensions were 50wt%, 55wt%, and 60wt%. The obtained homogeneous slurries were casted into plastic molds and then consolidated. After demolding, the green bodies were dried at room temperature for 48h. Finally, the samples were heated up to 600℃ in vacuum with a dwell time of 2h to remove organic additives followed by sintering at 1700℃ for 2h under N_2 atmosphere to obtain porous Si_3N_4 ceramics.

The as-received porous Si_3N_4 ceramics were immersed into 3- (Trimethoxysilyl) propyl methacrylate (KH-570, Sinopharm Chemical Reagent Co., Ltd., Shanghai, China) solution (the solvent was ethanol) with a concentration of 5 wt% for 3 h followed by a drying at 120℃. The silane-coupling agent treated samples were

subsequently immersed in the monomer solution of Methyl methacrylate (MMA, Huliang Biological Technology Co., Ltd., Shanghai, China) containing 1wt% benzoyl peroxide (BPO, Huliang Biological Technology Co., Ltd., Shanghai, China) for 24 h, followed by a polymerization procedure at 150℃ for 1 h under atmospheric pressure. Porous Si_3N_4 ceramics obtained from suspensions with solid content of 50wt%, 55wt%, 60wt% were named as SN50, SN55, SN60, respectively. Polymer-infiltrated Si_3N_4 composites obtained from SN50, SN55, SN60 were named as PSN50, PSN55, PSN60, respectively.

Fig. 1 illustrated the detailed procedure of polymer infiltrating in the present work. The elongated Si_3N_4 grains stacked together and resulted in well connected pores in porous ceramic scaffolds. As immersing porous Si_3N_4 scaffolds into PMMA resin, polymer monomers infiltrated into pores automatically due to the capillarity. After dwelling for certain time, pores in ceramic scaffolds were filled by polymer monomers. Then polymer infiltrated composites were fabricated by in-situ curing of PMMA.

2.2 Characterization of microstructure and mechanical properties

Morphologies of the samples were observed by scanning electron microscope (SEM, S-3400N, Hitachi, Japan). The back scattered electron (BSE) and corresponding energy dispersive spectrometer (EDS) images of PISNCs were observed by a field-emission scanning electron microscope (FE-SEM, SU8220, Hitachi, Japan). Porosity of porous Si_3N_4 ceramics and polymer-infiltrated Si_3N_4 ceramics were measured by Archimedes method. Flexural strength were tested via a

three-point bending method with a span of 30.0mm and a cross-head speed of 0.5mm·min^{-1} using specimens with dimensions of 3.0mm×4.0mm×36.0mm (Instron-5566, Instron Co., Ltd., American). The tensile surface was polished with diamond paste before testing. Five parallael samples of each composition were used for the measurements of flexural strength and open porosity. Micro-hardness measurements were carried out on a Vickers hardness tester (TUKON-2100B, Instron Co., Ltd., American) and the mean value was an average of five measurements.

2.3 Cytocompatibility

Sample treatment

PSN60 ceramic-polymer composite was selected as a representative polymer-infiltrated Si_3N_4 composite to evaluate the cytocompatibility and cytokine release behavior, compared with pure PMMA and Si_3N_4 samples. Surface of the samples were ground and polished to get a similar condition to clinical use. The polished samples were ultrasonically cleaned with ethonal, sterilized water and acetone in turn and then dried in air. Finally, all the samples were autoclaved at 150°C for 60 min.

Cell culture

Human gingival fibroblast cells (HGFs, Department of Orthopedics, Shanghai Sixth People's Hospital, Shanghai, China) were used to evaluate the cytocompatibility and IL-6 release. HGFs were cultured in a 5% CO_2 incubator at 37°C with the d-minimum essential medium (D-MEM, Gbico, Invitrogen Inc.) containing 10% fetal bovine serum (FBS, Hyclone, USA) and 1% antimicrobial of penicillin and

streptomycin (Hyclone, USA). Cell culture medium was changed every 2 days. Before reseeding cells on the sample surface, HGFs were detached from the 75cm^2 flakes with 1ml trypsin/EDTA (0.25% trypsin, 0.02% EDTA) (Gibco, Invitrogen) at 37°C with 5% CO_2 for one minutes followed by a centrifugation at 1000 rpm for 5 min. Then, the supernatant was removed and proper amount of DMEM was added to prepare cell suspentions with cell densities of 10.0×10^4 cells/ml and 5.0×10^4 cells/ml .

Cell morphology

The autoclaved samples were put in a 24-well culture plate and 1mL HGFs suspension with a cell density of 10.0×10^4 cells/ml were added to each sample. At each collecting time point, the samples with HGFs were transferred to a new 24-well plate and washed with phosphate buffered saline (PBS) for twice. Afterwrds, an overnight fixation in 2.5% glutaraldehyde was performed. The fixed samples were then dehydrated in a graded series of ethanol solutions (30, 50, 75, 90, 95 and 100 v/v %) and then dried in air. The cell morphology were then observed by SEM.

Cell proliferation

300 μl HGFs suspension with a cell density of 5.0×10^4 cells/ml were added to each sample and cultured for 2d, 5d and 7d. At each collecting time point, the samples were transferred to a new 96-well plate, then 150μl D-MEM of 10 v/v% alamar blue was added to each sample and cultured for another 2h. Afterwards, 100μl of the above medium was transferred into a 96-well black plate and the fluorescent intensity was measured with an excitation wavelength and emission wavelength of 560 nm and 590

nm, respectively.

Cytokine analysis

Samples were put into a 96-well culture plate. 300μl HGFs suspension with a cell density of 10.0×10^4/ml were added to each well and cultured for 6h, 1d, and 2d. At each collecting time point, the supernatant was collected and fresh culture medium was added. All the collected supernatant was stored at -20°C before testing. The amount of released IL-6 was investigated using ELISA test system according to the manufacturer's instructions (Human IL-6 Elisa Kit, Invitrogen, USA). The amount of cytokine release was quantified against a standard curve of purified human IL-6.

2.4 Statistical analysis

All data were expressed as mean ± standard deviation (SD). The statistically significant difference was measured using two-way analysis of variance and Tukey's multiple comparison tests. Statistical analysis was carried out using a GraphPad Prism 5 software package and the value of $p < 0.05$ was considered statistically significant.

3. Results

3.1 Porosity and mechanical performance of porous Si_3N_4 ceramics and PISNCs

Open porosity and flexural strength of the porous Si_3N_4 ceramics and PISNCs were shown in Fig. 2a-b. It could be seen that the porosity of Si_3N_4 scaffolds decreased slightly with the increase in Si_3N_4 content. Accordingly, the flexural strength showed an increace with the increase in Si_3N_4 content. All porous Si_3N_4 scaffolds possessed excellent mechanical strength with moderate porosity as expected. These high strength porous scaffolds guaranteed the excellent mechanical strength of PISNCs.

After polymer infiltrating process, nearly fully dense composites (with porosity less than 2.3%) could be obtained and the flexural strength was greatly improved. The flexural strength of PSN60 reached up to 385.3MPa. The hardness of PISNCs was less than 2.4GPa and the elastic modulus is less than 59.3MPa, which is similar to human bone tissues. It indicated that PISNCs possessed excellent flexural strength with moderate hardness and elastic modulus (Fig. 1c-d).

3.2 Microtopography of porous Si_3N_4 scaffolds and PISNCs

Fig. 3 showed the fracture surface of porous Si_3N_4 ceramic SN50 and its corresponding polymer-infiltrated composite PSN50. The micrographs revealed typical elongated Si_3N_4 grains in porous Si_3N_4 ceramic through liquid-phase-sintering mechanism[14]. After polymer was infiltrated, few pores were detected on the cross section of PSN50 sample, indicating a well infiltration of polymer and good combination of ceramic phase and polymer phase.

3.3 Surface elemental characterization of PISNCs

Element analysis of PSN50 were shown in Fig. 4. The back scattered electron (BSE) image in Fig. 4a revealed the possible distribution of ceramics and polymer phase by the difference between brightness. In the Fig. 4a, the white flakes represented the location of yttrium (Y) which was the heaviest element among the existed elements in the sample. The darkest part represented the the location of element carbon (C). Thus, the brighter parts showed area of element nitrogen (N). The energy dispersive spectrometer (EDS) results in Fig. 4b-d further confirmed the distribution of elements N, C and Y by direct pointed out the distribution of them on the surface. The three

elements could be regarded as references of Si_3N_4, PMMA and Y_2O_3, respectively. Thus the interpenetrated structure of ceramic skeleton and polymer were verified.

3.4 Response of HGFs

To be successfully used *in vivo*, the cytocompatibility of PSN60 were evaluated using HGFs. Pure medical PMMA and Si_3N_4 were used as controls. SEM morphologies of HGFs cultured on various surfaces at various time points were shown in Fig. 5. After 1h culture, HGFs on PMMA surface exhibited a spherical morphology with few filopodia, while the cells seeded on Si_3N_4 and PSN60 samples spread much faster than those on PMMA surface, both filopodia and lamellipodia could be clearly observed. With an increase of culture time, HGFs on Si_3N_4 and PSN60 samples showed polygonal sharps with plenty of filopodia and lamellipodia while the cells on PMMA just started to spread. After 24h culture, HGFs on all samples displayed a flat spreading with a lot of filopodia and lamellipodia. The cells on Si_3N_4 and PSN60 samples displayed much better adhesion than those on PMMA. The above results indicated that PSN60 samples enhanced the initial adhesion and spreading activity of HGFs compared with PMMA.

The proliferation of HGFs cultured on sample surfaces were estimated by the alamar blue assay and the results were shown in Fig. 6. At the early stage of culture, there were no statistically difference among the three groups. After 5 and 7 days culture, the cell proliferation on Si_3N_4 samples was slightly higher than that on PMMA and PSN60 samples, but the differences were not significant. In general, HGFs on all three samples showed a significantly increase with the increase in culture

time, indicating PSN60 and the control groups were all favorable to the growth and proliferation of HGFs.

IL-6 was generally regarded as one of the key cytokines which were involved in the induction and regulation of host responses in the inflammatory reactions[15]. In order to determine the early gingival and periodontal inflammation caused by the three kinds of materials, the release of IL-6 from HGFs was investigated and the results were shown in Fig. 7. In a whole, the IL-6 released at very low level for all the groups at all collecting time points. At all the collecting time points, Si_3N_4 sample showed a lower level of IL-6 release than PMMA and PSN60 samples, indicating Si_3N_4 ceramic had a superior biocompatibility. While the IL-6 release was no significant difference between PSN60 and PMMA samples. Thus the composite PSN60 were potential to have comparable biocompatibility with medical PMMA.

4. Discussion

Gelcasting has always been proved as a way to fabricate ceramics with uniform microstructure and excellent mechanical performance since reported by Omatete et al[16-18]. Generally, fabricating porous scaffolds with high strength were one of the most essential points to obtain polymer-infiltrated composites with excellent mechanical properties. Thus, porous Si_3N_4 ceramics fabricated through gelcasting that possessed high strength were promising candidates of porous scaffolds in polymer-infiltrated composites. Additionally, liquid-phase-sintered porous Si_3N_4 ceramics possessed porous structure by clubbed grain stacking [19-22]. Excellent connectivity between these pores was ensured by this unique microstructure, which

was important for fully infiltrating of polymer into pores. Thirdly, these elongated β-Si_3N_4 grains could lead to cracks deflection in fracture, which would be beneficial to the mechanical performance of the composites [23, 24]. In this work, porous Si_3N_4 ceramics with moderate porosity and excellent mechanical strength were fabricated by gelcasting method as shown in Fig. 2. Porosity as well as flexural strength were able to be adjusted by controlling solid content of suspensions in preparing procedure. With increasing solid content of suspensions from 50wt% to 60wt%, open porosity of porous Si_3N_4 ceramics decreased from 49.3% to 45.1%, while the flexural strength increased from 171.8MPa to 262.3MPa accordingly.

Polymer was infiltrated into porous Si_3N_4 scaffolds to fabricate PISNCs. Fig. 2(a) indicated that pores in scaffolds were well filled by polymer, the porosity of PISNCs was lowered to 1.94%-2.28%. An impressive improvement in flexural strength after compositing was also detected from Fig. 2(b). The PSN60 possessed flexural strength of 385.3±14.3MPa, which was much higher than commercially resin-based composites [11] and comparable with Si_3N_4-bioglass composites [25]. The comparison of different polymer-based composites, including the result of present study was shown in Fig. 8. It was attractive to find out that the polymer infiltrated Si_3N_4 composite showed super-high flexural strength. Generally, composites possessed flexural strength less than 200MPa, had limited applications. Polymer infiltrated zirconia and silicon nitride ceramics could lead to composites with flexural strength higher than 300MPa. Comparing to the polymer infiltrated zirconia composites with polymer content less than 30vol% [29], the polymer content in

PSN60 prepared in the present reached nearly up to 43vol%, which could result in a better machinability.

Moreover, the hardness of PISNCs ranged from 1.86GPa to 2.40GPa, which were similar to the hardness of enamel [26]. Once referred to elastic modulus, more potential could be expected for PISNCs. It was believed that high modulus of ceramics might lead to stress shielding in body. While the elastic modulus of PISNCs (52.1-56.1GPa) located closely to the modulus of cortical bone[25] and enamel[26], thus PISNCs could possess significant potentials in high load medical applications.

Micrographs of fracture surface from porous Si_3N_4 ceramics SN50 showed uniform distribution of Si_3N_4 grains and pores, which was important for the well mechanical performance of both porous scaffolds and PISNCs. These clubbed grains stacked together played essential roles in the high strength. After polymer infiltrating and curing, almost all pores were filled by polymer in Fig. 3b. However, several nano-pores were still existed in the composites, these pores were origined from pores failed to be infiltrated or caused by resin shrinkage. The detail distribution of polymer and ceramic phases in the bicontinuous PISNC was shown in Fig. 4. Elements distribution in Fig. 4b-d of N, C, Y represented the distribution of Si_3N_4, PMMA and Y_2O_3, respectively, which agreed well with what was seen from BSE image in Fig. 4a. The connected pores in ceramic was filled by polymer phase, constructed a bicontinuous organic-inorganic composite.

Although high strength PMMA-Si_3N_4 composites were obtained, it should be noted that some corner areas of pores formed by stacked grains in PISNCs were not fully

infiltrated in this study, which might because the special pore structure caused by rod shape Si_3N_4 grains. Thus the mechanical performance of PISNCs still had room for improvement. A schematic illustration of this phenomenon was shown in Fig. 9.

A schematic in Fig. 10 was used to explain this phenomenon through mechanical equilibrium. During the infiltrating, when polymer droplet infiltrated to the corner of stacked grains, a balance can be explained by the following equation:

$$F_i = F_p + 2\cos\theta F_f$$

where F_i is the force that pushing polymer forward, F_p is the force that caused by air left in the pores, F_f is the friction force between polymer and Si_3N_4 grains. Under this mechanical balance, polymer cannot fill the pores completely and results in unfilled pores in PISNCs. If F_i had advantages over other forces, polymers would further infiltrating until a new balance was reached. In fact, as long as air remained in the pores, a balance would be reached anyhow since F_p increased along with volume compression. Thus, these pores were hard to be infiltrated completely in porous scaffolds. To achieve idealy infiltrated composites, vacuum treatment before and during infiltrating could be a good additional assistance, which would benefitial to the further improvement of the mechanical performance.

The cytocompatibility results showed that PSN60 possessed excellent performance on initial adhesion, spreading and proliferation of HGFs. IL-6 release behavior in HGFs cultured with materials was used to predict the early gingival and periodontal inflammation stimulated by three groups of materials. It showed that the three groups exhibited low IL-6 release implying that all the tested materials had slight

inflammatory response. Since Si_3N_4 ceramic is a stable bioinert material, it showed a significantly lower level of IL-6 release than PMMA and PSN60 samples, indicating Si_3N_4 ceramic had an suprior biocompatibility. While, PSN60 showed a similar IL-6 release performance with PMMA. Since PMMA had been widely used in dental restorations, it indicated that PISNCs would be clinically safe.

5. Conclusions

In the present work, polymer-infiltrated Si_3N_4 composites with excellent mechanical performance were fabricated from high strength porous Si_3N_4 ceramics. PISNCs possessed excellent flexural strength with moderate hardness and elastic modulus. The flexural strength of PISNCs obtained from SN60 was high as 385.3MPa, which contained a polymer volume nearly 43 vol%. Whereas, the hardness and elastic modulus of PSN60 were 2.4GPa and 56.1GPa, respectively, which were close to those of enamel. The excellent mechanical properties of PISNCs should be attributed to the special pore structure formed by elongated Si_3N_4 grains and highly interconnected bicontinuous organic-inorganic microstructure. In addition, PISNCs also exhibited excellent biocompatibility on HGFs. PSN60 possessed excellent performance on initial adhesion, spreading and proliferation of HGFs, as well as a similar IL-6 release performance with PMMA. In conclusion, polymer-infiltrated Si_3N_4 composites are mechanical promising candidates for dental restorations and high-load medical applications.

Acknowledgments

This work was supported by Shanghai Committee of Science and Technology,

China (17441904100).

6. References

[1] FLR. Silicon Nitride and Related Materials. Journal of the American Ceramic Society. 2000;83:245–65. http://dx.doi.org/10.1111/j.1151-2916.2000.tb01182.x

[2] Jansen M. High Performance Non-Oxide Ceramics I: Springer Berlin Heidelberg; 2002. http://dx.doi.org/10.1007/3-540-45613-9

[3] Petzow G, Herrmann M. High Performance Non-Oxide Ceramics II: Springer Berlin Heidelberg; 2002. http://dx.doi.org/10.1007/3-540-45623-6_2

[4] HK. Silicon Nitride for High-Temperature Applications. Journal of the American Ceramic Society. 2010;93:1501–22. http://dx.doi.org/10.1111/j.1551-2916.2010.03839.x

[5] Bodišová K, Kašiarová M, Domanická M, Hnatko M, Lenčéš Z, Nováková ZV, et al. Porous silicon nitride ceramics designed for bone substitute applications. Ceramics International. 2013;39:8355–62. https://doi.org/10.1016/j.ceramint.2013.04.015

[6] Mazzocchi M, Bellosi A. On the possibility of silicon nitride as a ceramic for structural orthopaedic implants. Part I: processing, microstructure, mechanical properties, cytotoxicity. Journal of Materials Science: Materials in Medicine. 2008;19:2881-7. http://dx.doi.org/10.1007/s10856-008-3417-2

[7] Mazzocchi M, Gardini D, Traverso PL, Faga MG, Bellosi A. On the possibility of silicon nitride as a ceramic for structural orthopaedic implants. Part II: chemical stability and wear resistance in body environment. Journal of Materials Science: Materials in Medicine. 2008;19:2889-901. http://dx.doi.org/10.1007/s10856-008-3437-y

[8] Salgueiredo E, Vila M, Silva MA, Lopes MA, Santos JD, Costa FM, et al. Biocompatibility

evaluation of DLC-coated Si3N4 substrates for biomedical applications. Diamond & Related Materials. 2008;17:878-81. http://dx.doi.org/10.1016/j.diamond.2007.08.019

[9] Badran Z, Struillou X, Hughes F J, et al. Silicon Nitride (Si3N4) Implants: The Future of Dental Implantology? Journal of Oral Implantology, 2017; 43:240-244. http://dx.doi.org/10.1563/aaid-joi-D-16-00146

[10] Ilie N, Hickel R. Resin composite restorative materials. Australian Dental Journal. 2011;56 Suppl 1:59-66. http://dx.doi.org/10.1111/j.1834-7819.2010.01296.x

[11] Rodrigues Junior SA, Zanchi CH, Carvalho RV, Demarco FF. Flexural strength and modulus of elasticity of different types of resin-based composites. Brazilian Oral Research. 2007;21:16-21. http://dx.doi.org/10.1590/S1806-83242007000100003

[12] He LH, Swain M. A novel polymer infiltrated ceramic dental material. Dental Materials. 2011;27:527-34. https://doi.org/10.1016/j.dental.2011.02.002

[13] Wang F, Xiong Y, Ning C, et al. Effects of pore connectivity and microstructure on mechanical performance of ZrO2 scaffolds and PMMA-infiltrated ZrO2 composites. Journal of Alloys and Compounds, 2017;728:189-195. https://doi.org/10.1016/j.jallcom.2017.08.277

[14] Wang F, Gu H, Yin J, et al. Porous Si3N4 ceramics fabricated through a modified incomplete gelcasting and freeze-drying method. Ceramics International, 2017;43:14678-14682. https://doi.org/10.1016/j.ceramint.2017.07.194

[15] Schmalz G, Schuster U, Schweikl H. Influence of metals on IL-6 release in vitro. Biomaterials, 1998;19:1689-1694. https://doi.org/10.1016/S0142-9612(98)00075-1

[16] Young AC, Omatete OO, Janney MA, Menchhofer PA. Gelcasting of Alumina. Journal of the American Ceramic Society. 1991;74:612-8. http://dx.doi.org/10.1111/j.1151-2916.1991.tb04068.x

[17] Omatete OO, Janney MA, Nunn SD. Gelcasting: From laboratory development toward industrial production. Journal of the European Ceramic Society. 1997;17:407-13. https://doi.org/10.1016/S0955-2219(96)00147-1

[18] Wang F, Gu H, Yin J, et al. Porous Si3N4 fabrication via volume-controlled foaming and their sound absorption properties. Journal of Alloys and Compounds, 2017, 727: 163-167. https://doi.org/10.1016/j.jallcom.2017.07.232

[19] Li X, Zhang L, Yin X. Effect of chemical vapor infiltration of Si3N4 on the mechanical and dielectric properties of porous Si3N4 ceramic fabricated by a technique combining 3-D printing and pressureless sintering. Scripta Materialia. 2012;67:380-3. https://doi.org/10.1016/j.scriptamat.2012.05.030

[20] Yang JF, Deng ZY, Ohji T. Fabrication and characterisation of porous silicon nitride ceramics using Yb2O3 as sintering additive. Journal of the European Ceramic Society. 2003;23:371-8. https://doi.org/10.1016/S0955-2219(02)00175-9

[21] Li X, Wu P, Zhu D. Effect of foaming pressure on the properties of porous Si3N4 ceramic fabricated by a technique combining foaming and pressureless sintering. Scripta Materialia. 2013;68:877-80. https://doi.org/10.1016/j.scriptamat.2013.02.033

[22] Wang F, Yin J, Yao D, Xia Y, Zuo K, Liang H, et al. Effects of oil on gelcasting of oil-in-water Si3N4 suspensions. Journal of Alloys & Compounds. 2016. https://doi.org/10.1016/j.jallcom.2016.12.377

[23] Lu LM, Zuo KH, Zeng YP. Fabrication and properties of surface-modified β-Si3N4 whiskers reinforced dental resin composites. Journal of Applied Polymer Science. 2013;128:41-6. https://doi.org/10.1002/app.38125

[24] Bal BS, Rahaman MN. Orthopedic applications of silicon nitride ceramics. Acta Biomaterialia. 2012;8:2889. https://doi.org/10.1016/j.actbio.2012.04.031

[25] Amaral M, Lopes MA, Silva RF, Santos JD. Densification route and mechanical properties of Si3N4-bioglass biocomposites. Biomaterials. 2002;23:857. https://doi.org/10.1016/S0142-9612(01)00194-6

[26] Cuy JL, Mann AB, Livi KJ, Teaford MF, Weihs TP. Nanoindentation mapping of the mechanical properties of human molar tooth enamel. Archives of Oral Biology. 2002;47:281-91. https://doi.org/10.1016/S0003-9969(02)00006-7

[27] Garoushi S, Vallittu PK, Lassila LV. Short glass fiber reinforced restorative composite resin with semi-inter penetrating polymer network matrix. Dental Materials. 2007;23:1356-62. https://doi.org/10.1016/j.dental.2006.11.017

[28] Coldea A, Swain MV, Thiel N. Mechanical properties of polymer-infiltrated-ceramic-network materials. Dental Materials. 2013;29:419-26. https://doi.org/10.1016/j.dental.2013.01.002

[29] Li J, Cui BC, Lin YH, Deng XL, Li M, Nan CW. High strength and toughness in chromatic polymer-infiltrated zirconia ceramics. Dental Materials. 2016. https://doi.org/10.1016/j.dental.2016.09.003

[30] Ilie N, Hickel R. Resin composite restorative materials. Australian Dental Journal. 2011;56 Suppl 1:59-66. https://doi.org/10.1111/j.1834-7819.2010.01296.x

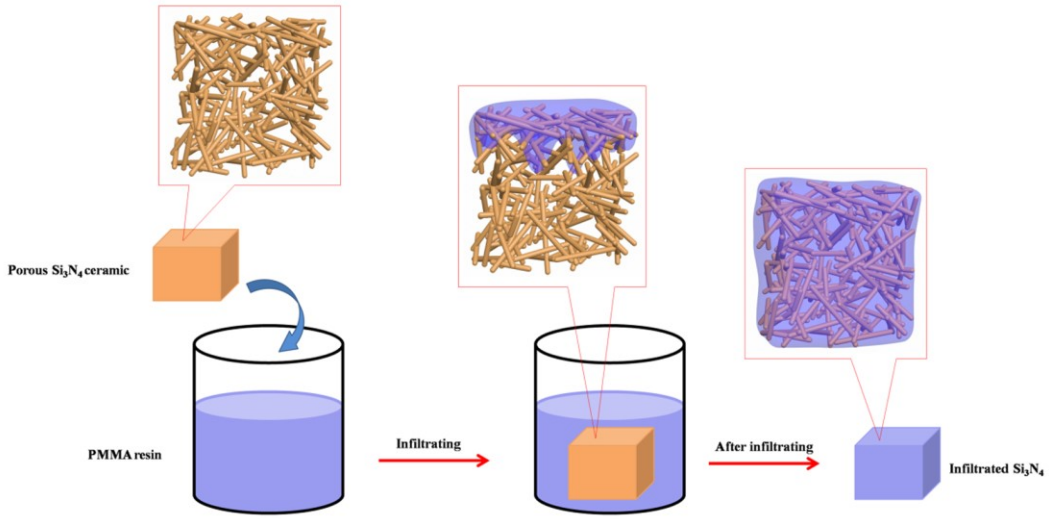

Fig. 1 Schematic illustration of polymer infiltrating procedure.

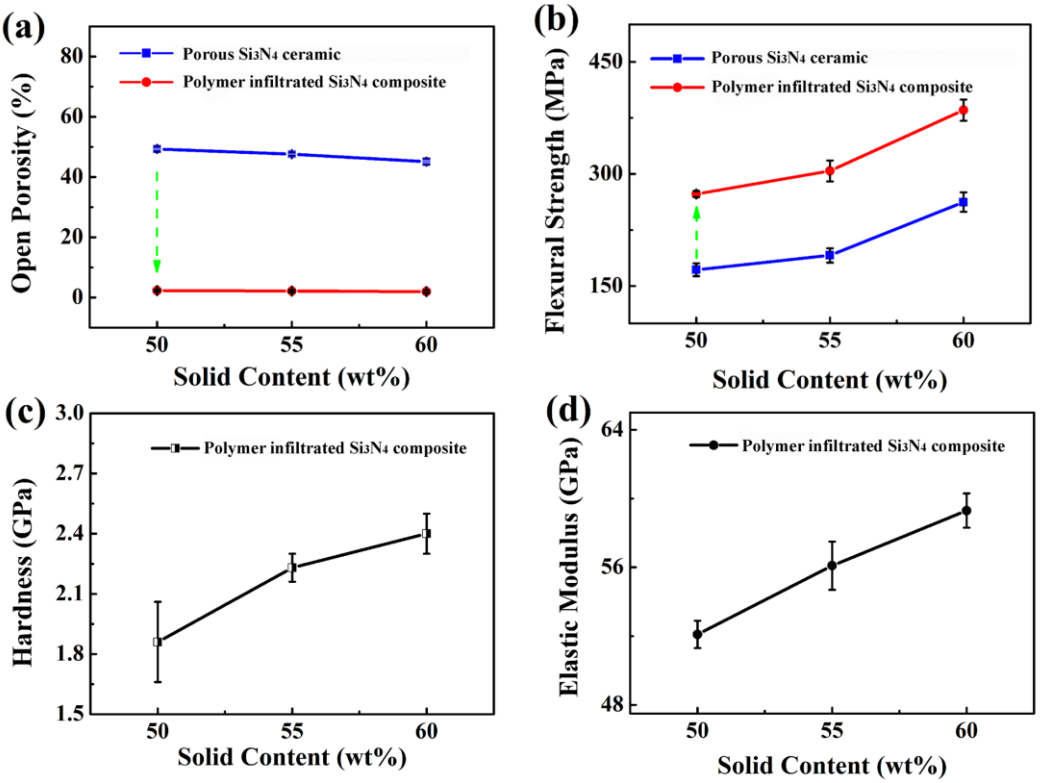

Fig. 2 Physical and mechanical properties of porous Si_3N_4 scaffolds and polymer infiltrated Si_3N_4 composites as a function of solid content: (a) open porosity, (b) flexural strength, (c) hardness, (d) elastic modulus.

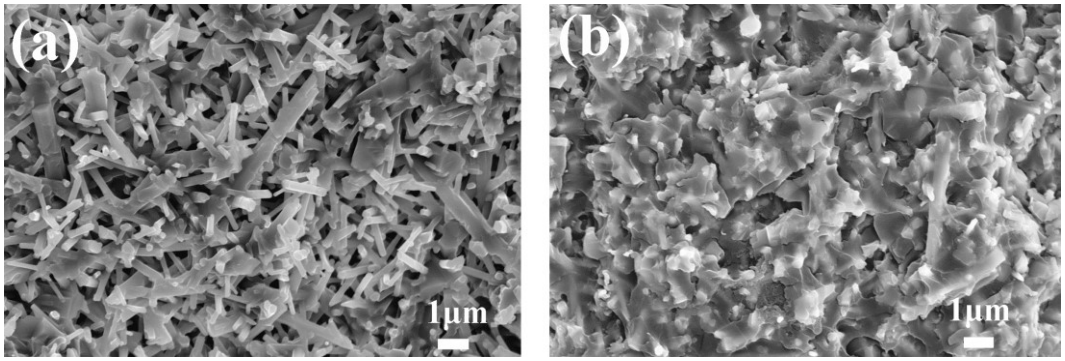

Fig. 3 Micrographs of fracture surface from porous Si_3N_4 ceramics SN50 (a) and polymer infiltrated Si_3N_4 ceramics PSN50 (b).

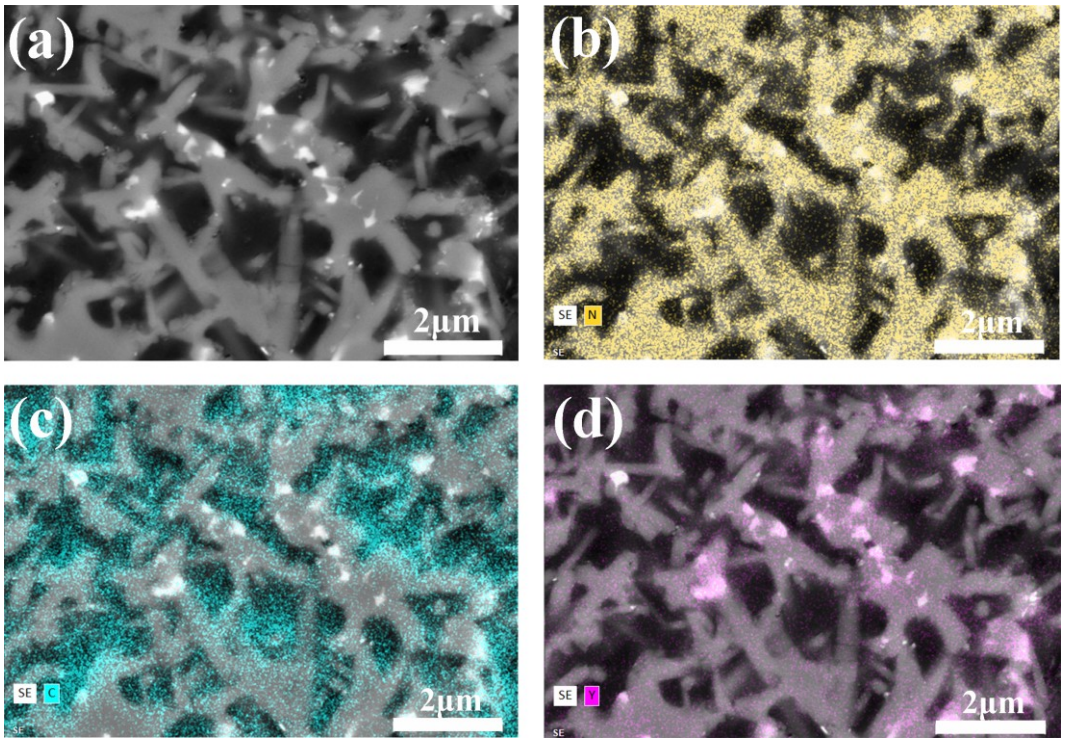

Fig. 4 The back scattered electron (BSE) and corresponding energy dispersive spectrometer (EDS) images of polymer infiltrated Si_3N_4 composite PSN50.

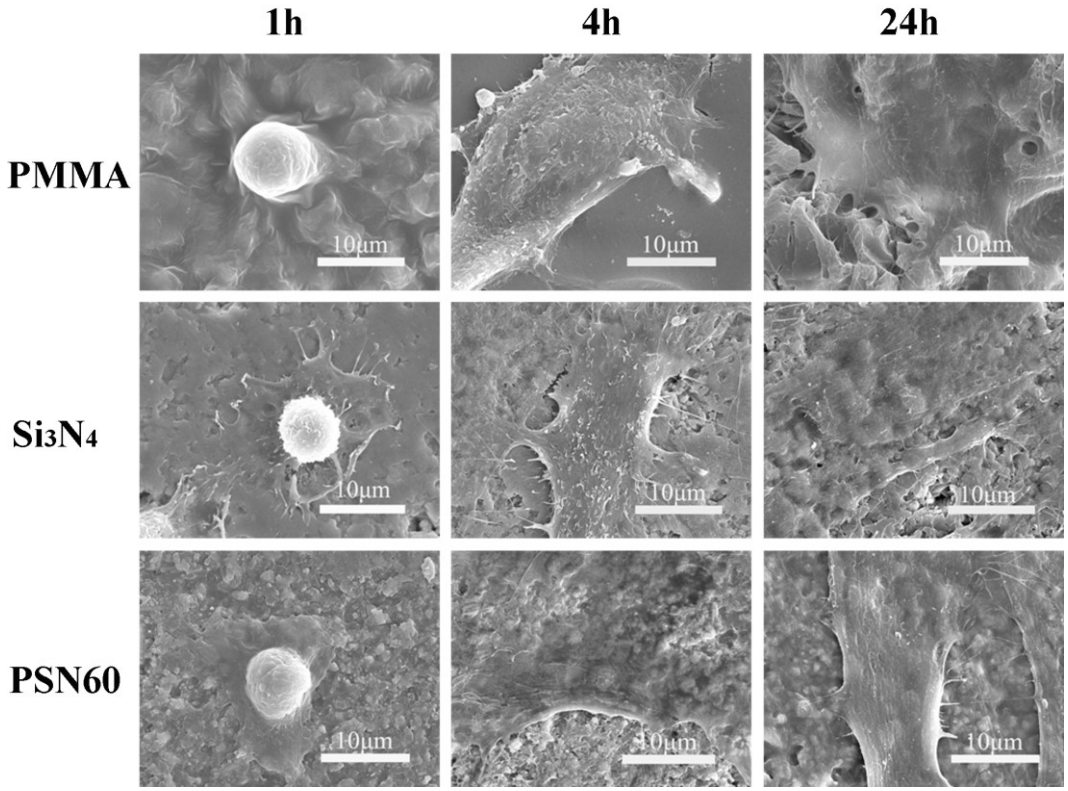

Fig. 5 SEM morphologies of HGFs cultured on sample surfaces for various times.

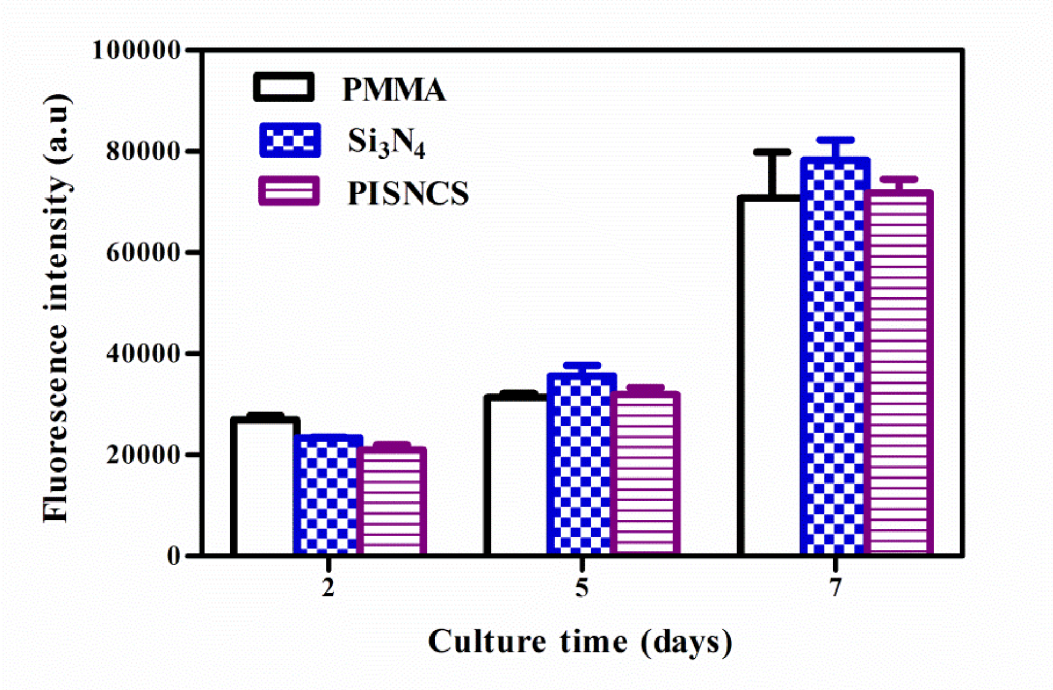

Fig. 6 Fluorescence intensity of HGFs cultured on sample surfaces for various times.

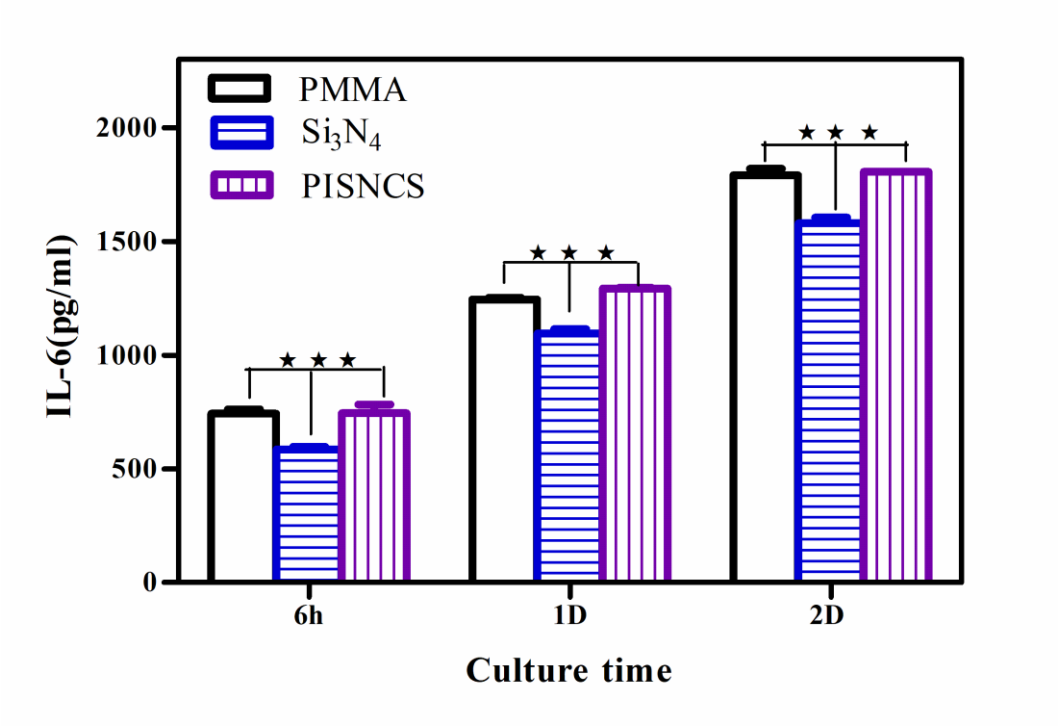

Fig. 7 IL-6 release of HGFs cultured on sample surfaces for various times, ***p < 0.001.

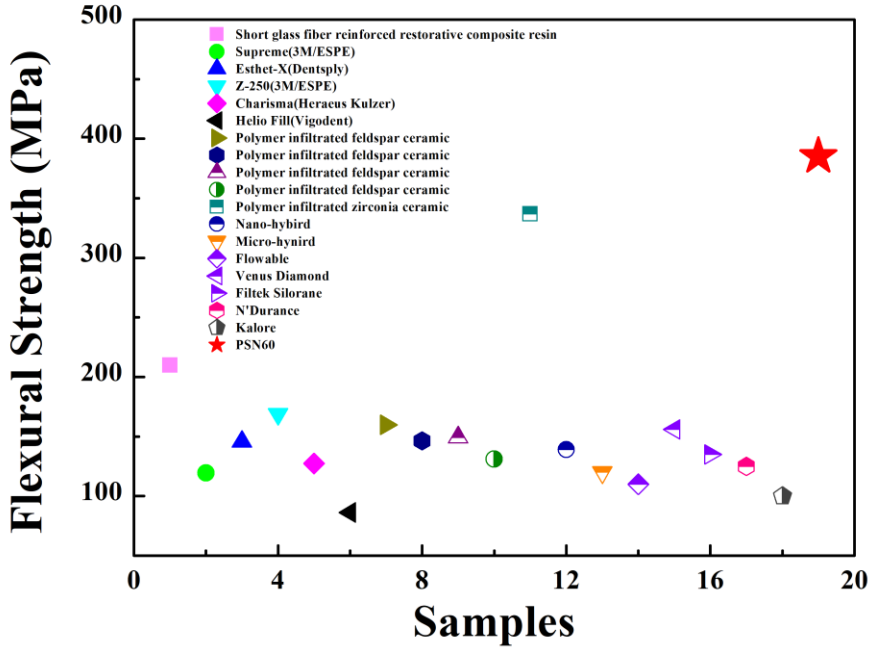

Fig. 8 Flexural strength of various organic-inorganic composites[11, 27-30]. The big red pentagram represents the flexural strength in this work.

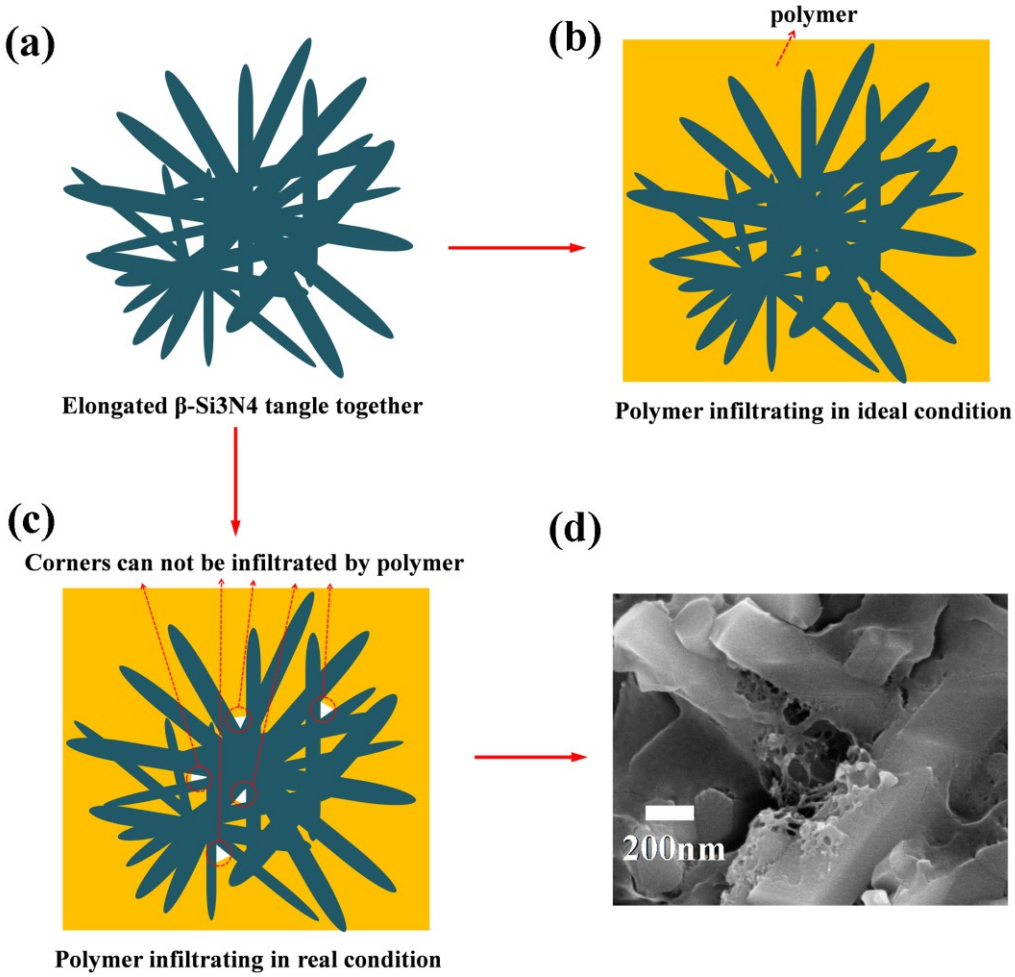

Fig. 9 Schematic illustration of polymer infiltrating in porous Si_3N_4 ceramics: (a)-(c). (d) shows corner area not fully infiltrated by polymer in the composite.

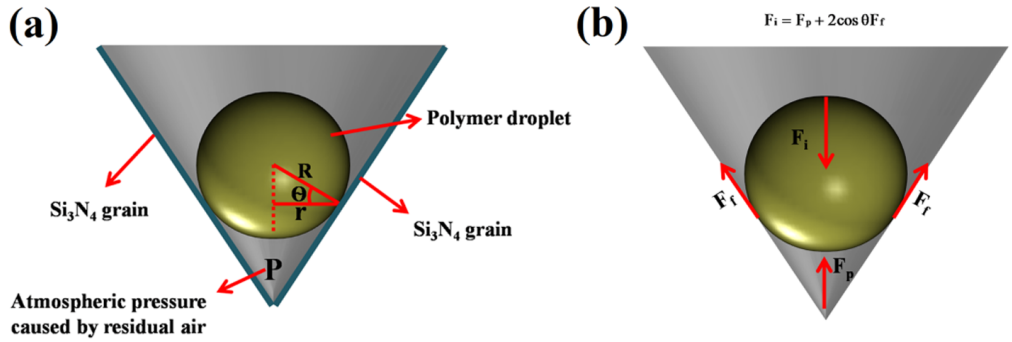

Fig. 10 Schematic illustration of force equilibrium during polymer infiltrating process in porous Si_3N_4 ceramics at corner areas.